Lyapunov indices with two nearby trajectories in a curved spacetime

X. Wu,[1,2,*] T.-Y. Huang,[2,†] and H. Zhang[2]

[1]*Department of Physics, Nanchang University, Nanchang 330047, China*
[2]*Department of Astronomy, Nanjing University, Nanjing 210093, China*
(Received 5 September 2005; revised manuscript received 19 July 2006; published 4 October 2006)

We compare three methods for computing invariant Lyapunov exponents (LEs) in general relativity. These methods involve the geodesic deviation vector technique (M1), the two-nearby-orbits method with projection operations and with coordinate time as the independant variable (M2), and the two-nearby-orbits method without projection operations and with proper time as the independent variable (M3). An analysis indicates that M1 and M3 do not need any projection operation. In general, the values of LEs from the three methods are almost the same. However, M2 fails for some specific cases. As a result, M3 is the most preferable to calculate LEs in most cases. In addition, we propose to construct the invariant fast Lyapunov indictor (FLI) with two-nearby-trajectories and give its algorithm in order to quickly distinguish chaos from order. Taking a static axisymmetric spacetime as a physical model, we apply different algorithms of the FLI to explore the global dynamics of phase space of the system where regions of chaos and order are clearly identified.

I. INTRODUCTION

Chaos is often visible in nonlinear systems. General relativity as a nonlinear theory is potentially chaotic. Although many features of chaos in Newtonian dynamics have been known clearly for over 40 years, their application in relativistic astrophysics began to be widely appreciated only within the last decade or so [1]. One main interest lies in studying the difference of dynamics between Newtonian and relativistic trajectories. Varadi *et al.* [2] noted that the general relativity effects are small for the outer planets but not negligible. Additionally, Wanex [3] revealed the chaotic amplification effect in the relativistic restricted three-body problem (namely, the ideal spacecraft-earth-moon orbital system). In particular, several authors found chaos in two relativistic systems including the two fixed black holes [4] and the Schwarzschild black hole plus a dipolar shell [5,6], which does not appear in their corresponding Newtonian counterparts at all. Another important problem that has been developed in recent years is to question whether spinning compact binaries [7–15] as promising sources of gravitational waves exhibit chaotic behavior because the gravitational-wave detection can not succeed when chaos is present. In practice, all the examples are attributed to the geodesic or nongeodesic motion of particles in a given gravitational field. On the other hand, the time evolution of the gravitational field itself, such as the mixmaster cosmology [4,16,17], is also of great interest.

In general, the methods for quantifying the ordered or chaotic nature of orbits in general relativity follow those widely applied in classical physics. Let us recall a fraction of these classical methods briefly. Poincaré's surface of section is one of the most common qualitative tools in the analysis of conservative Newtonian dynamical systems of not more than 2 degrees of freedom or with 3 degrees of freedom and axial symmetry. However, this technique is difficult to describe a higher dimensional phase space. Certainly, the principal Lyapunov exponent (LE), as a measure of the average exponential deviation of two nearby orbits, is frequently used. There are two different algorithms for the calculation of LE: the variational method and the two-particle one [18] (see Sec. II). The algorithm of LE is applicable to a phase space with any dimension, but a high dimension would cause extremely expensive computation to get a reliable value of LE. There are also other qualitative methods for multidimensional systems, such as the power spectra, smaller alignment index (SALI) [19,20] and fast Lyapunov indicators (FLIs) [21,22] etc. The power spectra display a finite number of discrete frequencies for regular orbits, whereas they are continuous for chaotic ones. One of its problems is that it is ambiguous to differentiate among complicated periodic orbits, quasiperiodic orbits and weakly chaotic orbits. As far as the SALI method is concerned, it is based on the difference or the sum of two normalized deviation vectors at the same points of an orbit. If the dimension of phase space is larger than 2, the indicator changes around nonzero values for regular orbits, while it tends exponentially to zero for chaotic orbits. The FLI uses the logarithm of the length of a deviation vector, which increases following completely different time rates for different orbits thus allowing one to distinguish between the ordered and chaotic cases (see Sec. III for some details). Both the SALI and the FLI are not only very fast tools to find chaos, but also can sketch out the global structure of phase space. Obviously it takes more CPU time for the former than for the latter since the former requires two deviation vectors, while the latter needs only one.

---

*Electronic address: xinwu@nju.edu.cn
†Electronic address: tyhuang@nju.edu.cn

Considering the above various cases, we are mainly in favor of applying two Lyapunov indices, the LE and the FLI, to study the geodesic or nongeodesic motion of particles in relativistic gravitational systems with at least 2 degrees of freedom. As is well known, the classical definition of LE depends on the choice of time and space coordinates in general relativity, because a coordinate gauge in relativity can be arbitrarily adopted so that time and space coordinates are not necessarily physical. In other words, there would be different values of the classical LEs in different coordinate systems. Even such LEs may provide wrong information on the dynamical features of a system. For instance, the maximum LE of a chaotic system turns out to be zero after a logarithmic time transformation, that is to say, chaos becomes hidden. Consequently, it is strongly desirable to develop a coordinate independent definition of LEs for the study of relativistic dynamics.

In general relativity, one can still follow the two approaches to calculate LEs as in the Newtonian case. As a counterpart of the variational technique, a geodesic deviation vector can be obtained from the geodesic deviation equation for a given geodesic flow in general relativity. Using it, one can easily get a method (M1) for the invariant LEs in the configuration space as well as in the phase space. In addition, Imponente and Montani [17] presented an invariant treatment by projecting a geodesic deviation vector for the Jacobi metric on an orthogonal tetradic basis. In this way they can succeed in gaining an insight into the dynamics of the mixmaster cosmology. On the contrary, it is seldom to see in the references that LEs are directly computed by use of the geodesic deviation equation. Perhaps it is rather troublesome to derive the complicated curvature tensor. In this sense, it is very natural to extend the two-particle method from the classical to the relativistic case. It is convenient to employ the method (M2) introduced by Wu and Huang [23]. They compute gauge invariant Lyapunov exponents by calculating the space separation between an ''observer'' and a ''neighbor'' particles that move along two neighboring orbits in the phase space. Here it is necessary to make use of a "1 + 3" split of the observer's spacetime and its space projected operator. Meanwhile, Wu and Huang [23] use coordinate time as the time variable of the equations of motion. Besides M2, there is another invariant two-particle method (M3), in which the integration time variables are the individual proper times of the two particles instead of the common coordinate time and the projection operation is not used. A method like M3 can be seen in many references (for example, see [8,12]) where the proper time and the Euclidian distance in the phase space are adopted, but we prefer to utilize the Riemannian distance in the configuration space than the Euclidian one in the phase space for conceptual clarity.

Tancredi *et al.* [24] have compared the two approaches for the calculation of LEs in Newtonian dynamics. It is still necessary to do a comparison of the three methods because

general relativity is much different from the Newtonian dynamics. A fundamental task is to select an optimal and valid algorithm to compute LEs. Another aim of our work is to provide a simple, rapid and efficient indicator of chaos which is independent of the dimension of phase space and the choice of time and space coordinates. It is assumed that this indicator not only can tell us some information about the global motion in a complicated multidimensional relativistic system, but also study the transition from regular motion to chaos as certain physical parameters alter.

In principle, it is possible to fulfill the two purposes in terms of LE. Udry and Pfenniger [25] made a detailed quantitative estimate of chaos in a series of 24 triaxial models of elliptical galaxies by means of LEs. They claimed that an interval of about 2 Hubble times corresponding to 66 periods or so is sufficient to get stable values of LEs for each of 100 randomly selected orbits in every model. However, as Contopoulos and Barbanis [26] found, lots of these orbits must be calculated for 12 500 periods, and sometimes up to 250 000 periods for the accomplishment of reliable values of LEs. On the basis of the values of the LEs, they displayed the structure of phase space of the systems. In addition, Caranicolas and Papadopoulos [27] studied the transition from regular motion to chaos in a 2-dimensional logarithmic potential of elliptical galaxies by observing the Poincaré surface of section as some dynamical parameters change. Of course, it is necessary to calculate thousands of orbits in the above cases, and each of them must be computed for long enough time in general. Consequently, the time required to compute such numbers is rather expensive, even would reach the limit of the present numerical experiments. Under these circumstances, one had better take advantage of the FLI as a quicker and more sensitive indicator to separate chaotic orbits from regular ones. As is mentioned above, the indicator is originally based on the tangential vectors from the variational equations of Newtonian dynamics [21]. Pondering the difficulty and complicacy to derive variational equations in general relativity, we shall be interested in developing the FLI method with the two particles approach—the FLI computed with two-nearby-orbits. It should be emphasized that this approach would meet difficulty without renormalization in the numerical calculation, different from the original approach of FLIs [21] with the tangential vector. An algorithm of FLI in the present paper will be provided.

This paper is organized as follows. The classical definition of LE is reviewed briefly, and the three methods M1, M2, and M3 in relativistic systems are introduced in Sec. II. Meanwhile, we offer a theoretical analysis of M1 and M3 to explain why they do not need projection operations. In addition, we discuss the scope of application of M2. In Sec. III the FLI with two nearby orbits and its algorithm are presented. Setting a static axisymmetric spacetime composed of a Schwarzchild black hole and an

octopolar shell as a test model, we investigate the global dynamics of this system. Finally, the summary follows in Sec. IV.

Throughout the work we use units $c = G = 1$, and take the signature of the metric as $(-, +, +, +)$. Greek subscripts run from 0 to 3 and Latin indexes from 1 to 3. The symbol $\circ$ denotes the Euclidian inner product; while $|\boldsymbol{a}|$ is the length of the vector $\boldsymbol{a}$ in the Euclidian space. The symbol $|a|$ represents the absolute value of a scalar a. In addition, $\bullet$ stands for the Riemannian inner product, and $\| \boldsymbol{\xi} \|$ is the Riemannian norm of the vector $\boldsymbol{\xi}$ corresponding to the tensor ξ^{α} or ξ_{α}. $\boldsymbol{f}$ is a set of functions. We specify t as a time coordinate variable, and τ, a proper time variable. $D/D\tau$ denotes a covariant derivative operator vs τ.

II. COMPARISONS OF THREE METHODS FOR COMPUTING LE IN GENERAL RELATIVITY

A. LE in classical physics

In classical physics the LE is to characterize the mean exponential rate of divergence of trajectories surrounding a given trajectory in the phase space. For a compact autonomous n-dimensional system

$$\dot{X} = f(X) \tag{1}$$

with the solution $X(t) = (x, \dot{x})$ and its corresponding variational equation

$$\dot{Y}(t) = \frac{\partial f}{\partial X} \circ Y \tag{2}$$

with a solution $Y(t) = (\boldsymbol{\xi}, \dot{\boldsymbol{\xi}})$ at time t, the maximum LE is given by

$$\gamma_1 = \lim_{t \to \infty} \frac{1}{t} \ln \frac{|Y(t)|}{|Y(0)|}. \tag{3}$$

This is called as the variational method. The system is chaotic if $\gamma_1 > 0$, otherwise it is regular. This way is rigorous to get the tangent vector $Y(t)$, but it is rather cumbersome to derive Eq. (2) in general. Because of that people usually use the deviation vector $\Delta X(t)$ between a reference trajectory $X(t)$ and a shadow one $\tilde{X}(t)$ as the approximate tangent vector. This is a less rigorous but still useful technique, so-called the two-particle method [18,24] or two-nearby-trajectories method, in which the LE in the expression of Eq. (3) is to be replaced by

$$\gamma_2 = \lim_{t \to \infty} \frac{1}{t} \ln \frac{|\Delta X(t)|}{|\Delta X(0)|}. \tag{4}$$

Here an initial separation $|\Delta X(0)|$ relative to $|X(0)|$ not larger than 10^{-8} is viewed as the best choice to guarantee ΔX as a good approximation to Y and to avoid the overestimation of LE [24].

As was mentioned in Ref. [23], it is preferable to compute the LE in the configuration space instead of in the phase space as LEs in the two spaces are both effective in detecting the long-term dynamical behavior of orbits. In this case, Eqs. (3) and (4) are, respectively, modified as follows

$$\lambda_1 = \lim_{t \to \infty} \frac{1}{t} \ln \frac{|\boldsymbol{\xi}(t)|}{|\boldsymbol{\xi}(0)|}, \tag{5}$$

$$\lambda_2 = \lim_{t \to \infty} \frac{1}{t} \ln \frac{|\Delta \boldsymbol{x}(t)|}{|\Delta \boldsymbol{x}(0)|}. \tag{6}$$

For the two particles method, it is necessary to scale the distance $|\Delta \boldsymbol{x}(t)|$ down from time to time. In this way, the shadow trajectory returns to the neighborhood of the reference one along the deviation vector $\Delta \boldsymbol{x}(t)$. The magnitude of $\Delta \boldsymbol{x}(t)$ shrinks to the initial distance $|\Delta \boldsymbol{x}(0)|$ after each renormalization, and the velocity deviation vector $\Delta \dot{\boldsymbol{x}}(t)$ should be multiplied by the same factor $|\Delta \boldsymbol{x}(0)|/|\Delta \boldsymbol{x}(t)|$. Meanwhile, it is also vital to avoid saturation of orbits in a bounded chaotic region.

The time t and coordinate x in Eq. (5) or Eq. (6) are not necessary physical and meaningful in general relativity. Thus, it is desirable to define covariant LE.

B. LEs in general relativity

For a given 4-dimensional spacetime with the metric $ds^2 = g_{\mu\nu}dx^{\mu}dx^{\nu}$, first we consider a rigorous definition of LEs by using a geodesic deviation vector.

1. Geodesic deviation vector technique

In the spacetime, a free particle moves along the geodesic equation $DU^{\mu}/D\tau = 0$, that is to say,

$$\ddot{x}^{\mu} = -\Gamma^{\mu}_{\alpha\beta}\dot{x}^{\alpha}\dot{x}^{\beta}, \tag{7}$$

and its geodesic deviation equation is

$$\frac{D^2\xi^{\mu}}{D\tau^2} = -R^{\mu}_{\alpha\lambda\beta}\xi^{\lambda}U^{\alpha}U^{\beta}, \tag{8}$$

where $\Gamma^{\mu}_{\alpha\beta}$, $U^{\alpha}(= \dot{x}^{\alpha})$, and $R^{\mu}_{\alpha\lambda\beta}$ stand for the Christoffel symbol, 4-velocity, and the Riemannian curvature tensor, respectively.

From Eq. (5), it is easy to get an invariant definition of LE if the Riemannian norm and proper time τ substitute the Euclidian norm and coordinate time t, respectively. In the geodesic deviation vector method (M1) the LE is given in the form

$$\Lambda_1 = \lim_{\tau \to \infty} \frac{1}{\tau} \ln \frac{\| \boldsymbol{\xi}(\tau) \|}{\| \boldsymbol{\xi}(0) \|}, \tag{9}$$

$$\| \boldsymbol{\xi}(\tau) \| = \sqrt{|\boldsymbol{\xi} \bullet \boldsymbol{\xi}|} = \sqrt{|g_{\mu\nu}\xi^{\mu}\xi^{\nu}|}. \tag{10}$$

As an illustration, a similar method given in the phase space can be seen in Ref. [28]. It is easily shown that the Riemannian inner product $\boldsymbol{\xi} \bullet \boldsymbol{\xi}$ is positive definite be-

cause $\boldsymbol{\xi}(\tau)$ is always spacelike when $\boldsymbol{\xi}(0)$ is spacelike for a given geodesic flow.

On the other hand, there is not a variational equation like the form (8) for a nongeodesic flow. However, it is still possible to derive the variational equation similar to Eq. (2) for the nongeodesic flow. For example, Nieto *et al.* [29] gave a relativistic top deviation equation as a generalization of the geodesic deviation equation for a pair of nearby point particles. Thus M1 remains valid if the spacetime background is $ds^2 = g_{\mu\nu}dx^\mu dx^\nu$.

2. Two-nearby-orbits method with projection operations

The derivation of the geodesic deviation equation is usually a rather hard task. In particular, it is much arduous to obtain the variational equation of a nongeodesic flow. Thus, it is a good idea to refine the classical definition by Eq. (6) using an invariant version of it, introduced by Wu and Huang [23] (method M2).

Let two particles, an observer and his "neighbor," move on two nearby- trajectories in a curved spacetime. At a coordinate time t the observer is at the point O with coordinate x^α and 4-velocity U^α, and his neighbor reaches the point $\tilde{O}$ with coordinate $\tilde{x}^\alpha$. The deviation vector

$$\Delta\boldsymbol{x}(t) = \Delta x^\alpha(t) = \tilde{x}^\alpha(t) - x^\alpha(t) \qquad (11)$$

from O to $\tilde{O}$ is projected to the observer's local space and the resulting projected vector is $\Delta x^\alpha_\perp = h^\alpha_\beta \Delta x^\beta$, where $h^{\alpha\beta} = g^{\alpha\beta} + U^\alpha U^\beta$ is the space projection operator of the observer. The space distance of the neighbor measured by the observer at time t is

$$\Delta L = \sqrt{g_{\alpha\beta}\Delta x^\alpha_\perp \Delta x^\beta_\perp} = \sqrt{h_{\alpha\beta}\Delta x^\alpha \Delta x^\beta}. \qquad (12)$$

Hence we define an invariant LE (M2) as

$$\Lambda_2 = \lim_{\tau\to\infty} \frac{1}{\tau} \ln\frac{\Delta L(\tau)}{\Delta L(0)}, \qquad (13)$$

where the proper time τ corresponds to the coordinate time t according to the metric. Obviously, this LE is independent of coordinate transformations [23].

There are detailed implementations of M2 in [23]. Here we emphasize that the coordinate time is adopted as the common independent variable for both particles in their equations of motion and one has to construct an equation for $d\tau/dt$, which is to be integrated together with the motion equations to get the proper time of the observer. The reason for doing this is that the two particles have their own and different proper times but the numerical integration demands a common time variable.

3. Two-nearby-orbits method without projection operations

On the other hand, if we integrate directly the equations of motion, Eq. (7), for two slightly distinct initial condi-

tions with the proper time as an integration variable, we attain the deviation vector

$$\Delta\boldsymbol{x}(\tau) = \Delta x^\alpha(\tau) = \tilde{x}^\alpha(\tau) - x^\alpha(\tau) \qquad (14)$$

at the proper time τ of the observer. Here a difference between Eq. (11) and (14) should not be neglected. The difference is that $\Delta\boldsymbol{x}$ is a function of t in Eq. (11), while being a function of τ in Eq. (14). In this case, we can give another two-nearby-orbits method (M3) as follows:

$$\Lambda_3 = \lim_{\tau\to\infty} \frac{1}{\tau} \ln\frac{\| \Delta\boldsymbol{x}(\tau) \|}{\| \Delta\boldsymbol{x}(0) \|}, \qquad (15)$$

$$\| \Delta\boldsymbol{x}(\tau) \| = \sqrt{|\Delta\boldsymbol{x} \bullet \Delta\boldsymbol{x}|} = \sqrt{|g_{\mu\nu}\Delta x^\mu \Delta x^\nu|}. \qquad (16)$$

Next let us study the three methods from the theoretical and numerical points of view.

C. The reason why M1 and M3 do not need projection operations

Obviously, projection operations do not appear in M1. Similarly, Hartl noted this fact in his Ph.D. thesis [8]. Now, we give a discussion on this issue. It has been shown without any difficulty that $\boldsymbol{\xi}(\tau)$ is always perpendicular to the 4-velocity $\boldsymbol{U}(\tau)$ at any (proper) time provided that $\boldsymbol{\xi}(0)$ and $D\boldsymbol{\xi}(0)/D\tau$ are both perpendicular to $\boldsymbol{U}(0)$, respectively [28]. What would happen if $\boldsymbol{\xi}(0) \bullet \boldsymbol{U}(0) \neq 0$ or $D\boldsymbol{\xi}(0)/D\tau \bullet \boldsymbol{U}(0) \neq 0$? Let us explore the question in the following.

Noting that $\boldsymbol{\xi} \bullet \boldsymbol{U}$ and $D\boldsymbol{\xi}/D\tau \bullet \boldsymbol{U}$ are scalars, we can operate a covariant derivative in place of an ordinary one. The demonstration is

$$\frac{d}{d\tau}(\boldsymbol{\xi} \bullet \boldsymbol{U}) = \frac{D}{D\tau}(\boldsymbol{\xi} \bullet \boldsymbol{U}) = \frac{D\boldsymbol{\xi}}{D\tau} \bullet \boldsymbol{U} + \boldsymbol{\xi} \bullet \frac{D\boldsymbol{U}}{D\tau}$$
$$= \frac{D\boldsymbol{\xi}}{D\tau} \bullet \boldsymbol{U}, \qquad (17)$$

$$\frac{d}{d\tau}\left(\frac{D\boldsymbol{\xi}}{D\tau} \bullet \boldsymbol{U}\right) = \boldsymbol{U} \bullet \frac{D^2\boldsymbol{\xi}}{D\tau^2} = -R^\mu_{\alpha\lambda\beta}\xi^\lambda U^\alpha U^\beta U_\mu$$
$$= -R_{\nu\alpha\lambda\beta}U^\alpha U^\beta U^\nu \xi^\lambda. \qquad (18)$$

The result of Eq. (18) is obviously identical to zero because it is both symmetric and antisymmetric with respect to the indicies ν and α. Consequently, it can be inferred that the right side of Eq. (17) is a constant C, which turns out to be the value of $D\boldsymbol{\xi}(0)/D\tau \bullet \boldsymbol{U}(0)$. As was stated above, $\boldsymbol{\xi} \bullet \boldsymbol{U} \equiv 0$ if $C = 0$. Otherwise we have

$$\boldsymbol{\xi} \bullet \boldsymbol{U} = C\tau + \tilde{C}, \qquad (19)$$

where $\tilde{C}$ is another constant corresponding to the initial value of $\boldsymbol{\xi} \bullet \boldsymbol{U}$. Now let us investigate the physical significance of $|\boldsymbol{\xi} \bullet \boldsymbol{U}|$. Obviously it is no other than the length of the projected vector $-(\boldsymbol{\xi} \bullet \boldsymbol{U})\boldsymbol{U}$, the time component of $\boldsymbol{\xi}$ as measured by the particle. Equation (19) shows that the

evolution of ξ along the time direction of the particle is linear, therefore, the LE in this direction vanishes. In fact, the result is very naturally due to the integral $U_\alpha U^\alpha = -1$. Therefore, ξ and its projected vector along the space direction of the particle change at the same rate with its proper time. This implies that it is not necessary to project ξ into the space direction in the calculation of the principal LE. In other words, it is reasonable to use M1 as the standard definition of the maximum LE in general relativity.

As to M3, the deviation vector $\Delta x(\tau)$ in Eq. (14) is viewed as an approximation to the geodesic deviation vector ξ by Eq. (8). Therefore, M3 is nearly the same as M1 as long as the length of ξ is kept small enough.

For M2, we use the projected vector $\Delta x_\perp^\alpha$ rather than $\Delta x(t)$ used in Eq. (11) as an approximation of ξ. $\Delta x(t)$ in Eq. (11) is the deviation vector between the observer and his neighbor at the same coordinate time t, therefore it is necessary for $\Delta x(t)$ to be projected along the space direction of the observer. On the other hand, $\Delta x(t)$ and U do not necessarily obey the relation (19) when t and τ have large difference. Then in the observer's in-track direction he may find LE in the form

$$\lambda_{\text{in-track}} = \lim_{\tau \to \infty} \frac{1}{\tau} \ln \frac{\Delta T(\tau)}{\Delta T(0)}, \qquad (20)$$

where $\Delta T(\tau) = |\Delta x(t) \bullet U|$ is the projection of $\Delta x(t)$ along the observer's time direction. This shows that one may find chaos in the observer's time direction if $\lambda_{\text{in-track}}$ is used as an index for chaos. This displays it necessary to employ the projection norm for M2.

We shall check the validity of the three methods through practical calculations further.

D. Scope of application of M2

Let us take a Weyl spacetime as a physical model (see the appendix), and choose parameters as $E = 0.9679$, $L = 3.8$, and $\mathcal{O} = 7.012 \times 10^{-7}$. The initial conditions of two variables r and $\dot{r}$ are arbitrarily given within their respective admissible intervals except $\theta = \pi/2$, while $\dot{\theta}$ is derived from Eq. (A4). First order differential systems from the geodesic Eqs. (A5) and (A6) are computed with a 7–8 order Runge-Kutta-Fehlberg algorithm of variable time-step [RKF7(8)]. A proper time output interval is 0.1, and the Poincaré surface of section is at the plane $\theta = \frac{\pi}{2}$ ($\dot{\theta} < 0$) in Fig. 1. The intersections of the orbits by this Poincaré surface of section describe the global dynamical feature of the system. There are two regions in the $(r, \dot{r})$ plane. One region with randomly distributed points is regarded as a chaotic one, while the other, a regular one consisting of many tori and islands.

Next we shall quantitatively describe the dynamics of particles moving in this spacetime by employing the LEs above.
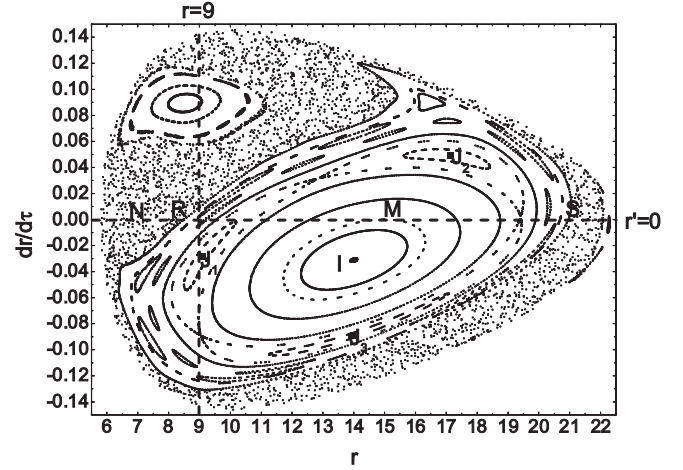

FIG. 1. Poincaré surface of section at the plane $\theta = \frac{\pi}{2}$ ($\dot{\theta} < 0$) for the full relativistic core-shell configuration consisting of a Schwarzschild black hole and a purely octopolar shell with parameters $E = 0.9679$, $L = 3.8$, and $\mathcal{O} = 7.012 \times 10^{-7}$.

For M1, it is necessary to integrate the dynamical Eqs. (A2)–(A6) numerically with their geodesic deviation equations together so that we obtain their solution (x^α, U^α) and their variational solution $(\xi, \dot{\xi})$ in the forms $\xi = (\delta t, \delta r, \delta \theta, \delta \phi)$ and $\dot{\xi} = (\delta \dot{t}, \delta \dot{r}, \delta \dot{\theta}, \delta \dot{\phi})$. Here the proper time τ is chosen as an integration variable. In addition, the renormalization technique is used if necessary. As far as M2 is concerned, we numerically trace the trajectories of the observer and his neighbor with the Eqs. (A7) and (A8) and the equations involving $d\tau/dt$ and $d\phi/dt$ with slightly different initial conditions. The initial conditions of the observer are the same as the above. As to his neighbor, an initial separation in the order of 10^{-8} is adopted only on the r direction, regarded as the best choice [24], and the other coordinates remain the same as the observer's except $\dot{\theta}$. This process also fits M3, but only Eqs. (A2)–(A6) are integrated numerically.

Choosing many ordered and chaotic orbits as numerical tests, we found that the three methods M1, M2 and M3 almost give the same final values of LEs for each orbit. There are only a few differences on the transition phases of the orbits. However, we found that M2 is not suitable for the study of some specific trajectories.

As a further test, we choose a chaotic orbit with the initial conditions: $t = 0$, $\theta = \pi/2$, $r = 9$, $\phi = 0$, $\dot{r} = 0.025$, and the initial value of $\dot{\theta}$ derived from Eq. (A4). Let the initial deviation vector satisfy $\delta t = \delta \theta = \delta \phi = \delta \dot{r} = \delta \dot{\theta} = 0$ and $\delta r = 1/\sqrt{g_{11}}$. As is shown in Fig. 2, M1 (A) is very close to M3 (C). Whereas the curve B does not converge at a certain value. This means the absence of a limit in Eq. (13), i.e. the failure of M2.

Here we give an explanation to the above puzzle. For the ordered orbit with the starting point $M(15, 0)$ in the plane $r - \dot{r}$ or the chaotic one with the initial point $N(7, 0)$, it can be found that the observer's proper time τ runs about 9.2×10^5 when t passes through 10^6, namely $\tau \approx t$. But in
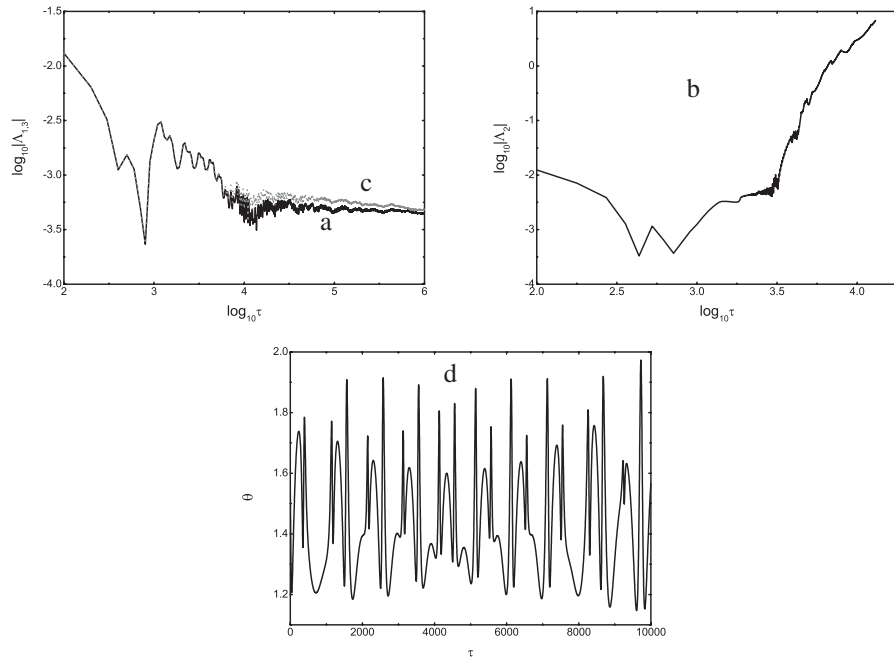
FIG. 2.   LEs for a chaotic orbit with the initial conditions $r = 9$ and $\dot{r} = 0.025$. (a) (M1) coincides nearly with (c) (M3), and (b) describes the failure of M2 for computing LEs. (d) denotes the domain admissible for the motion of θ, as an interpretation for an obstacle to the application of M2. For more details, see the text.

Fig. 2(b) τ spans 10^4 or so when t runs 10^6. In other words, the coordinate clock runs too fast so that M2 becomes useless. On the contrary, M2 is still successful in Ref. [23] although τ reaches only about 9.168×10^5 when the coordinate time η is equal to 10^7 even 10^9 (see Fig. 3 in [23]). In practice, the two aspects are not paradoxical. Here is a detailed analysis. For the observer, Eq. (A2) is rewritten as $d\tau/dt = [(r - 2)/r/E]e^P$. On the basis of the above background, we know that $(r - 2)/r/E \approx 1$. Thus $d\tau/dt \approx e^P$. In the case $P \equiv 0$, M2 is explicitly valid in the spacetime (A1) that corresponds to a Schwarzschild field. For a system consisting of a black hole plus a dipolar shell with $P = 2\mathcal{D}uv$ ($\mathcal{D}$, a positive dipolar parameter) [5], the sign of $d\tau/dt - 1$ changes frequently. Although there is a much larger t corresponding to a smaller τ from a long-time point of view, M2 is still significant. Now recalling our problem above, we can easily infer that P keeps the same sign as $v(5v^2 - 3)$. Assume $P \le 0$, then we can get $\arccos\sqrt{0.6} \le \theta \le \pi - \arccos\sqrt{0.6}$ (i.e. $\theta \in [0.68, 2.46]$) without any difficulty. The practical calculation in Fig. 2(d) gives $\theta \in (1, 2) \subset [0.68, 2.46]$. This seems to show that $d\tau/dt$ has an *exponential decay* (note: the decay relation seems to be described as $d\tau = e^{-F(t)}dt$, where $F(t) > 0$.) so that τ grows much more slowly than t although τ is a monotone increasing function of t. In addition, there are some key effects from numerical errors. All these factors may lead to the invalidity of M2.

For conceptual clarity it is of the physical significance to define LE as a coordinate gauge invariant in general rela-tivity. For this purpose, there are the above three methods (M1, M2 and M3) to compute LEs. M1 is more rigorous than M2 or M3. On the contrary, M2 is more convenient to use than M1, and M3 is the simplest. In addition, M2 and M3 are easier to treat a nongeodesic flow as well as a geodesic flow than M1. Numerical experiments display that M1, M2, and M3 not only can obtain the same final values but also have small differences in the transition phase for the calculation of LEs. In addition, we found that M2 fails for some orbits. Considering the application of convenience and validity, we conclude that M3 should be the most preferable and is worth to be recommended for the calculation of LE in a relativistic gravitational system in most cases. It is useful to accept some advice on a proper choice of the initial separation and a renormalization time step introduced by Tancredi *et al.* [24].

Although the LEs have been widely used to distinguish between regular and chaotic orbits, especially for systems with more than 2 degrees of freedom, they are not easy to use to explore the global structure of phase space. In view of this fact, we shall modify M3 and adopt its corresponding FLI in the following section.

III. DESCRIPTION OF THE STRUCTURE OF PHASE SPACE BY USING FLI WITH TWO-NEARBY-TRAJECTORIES

A. Fast Lyapunov indicators

The time interval that is necessary to reach a given value of either the length of a tangential vector or the angle

between two tangential vectors can be taken as an indicator of stochasticity of a Newtonian dynamical system. Following this idea, Froeschlé *et al.* [21] defined three different FLIs in 1997. However two of these methods need to solve the variational Eq. (2) for n times when a set of n independent initial tangential vectors with the same initial conditions are chosen. In this circumstance, Froeschlé and Lega [22] improved the FLI as follows

$$\psi(t) = \ln|Y(t)|, \qquad (21)$$

where Y is a tangential vector from Eq. (2) and $|Y(0)| = 1$. Given a threshold, the indicator ψ reaches a value fast for a chaotic orbit, but it would take a rather long time for an ordered one. Conversely, in the same time interval the indicator tends to different values for ordered and chaotic orbits. Namely it grows exponentially with time for the chaotic orbit, but only algebraically with time in the regular case. This allows one to distinguish between the two cases. There is a close relation between the FLI (ψ) and the LE [Eq. (3)]: the FLI divided by time t tends to the LE when the time is sufficiently large. Besides, overflow of the lengths of tangential vectors in the case of a chaotic orbit can be avoided because the integration time is not long enough. This is the reason why the indicator is classified as a "fast" method.

Following the idea above and the coordinate gauge invariance, in a curved spacetime we could easily define an invariant FLI corresponding to the LE in Eqs. (9) and (15). As far as the geodesic deviation vector method M1 is concerned, its corresponding FLI is

$$\Psi(\tau) = \log_{10} \| \boldsymbol{\xi}(\tau) \| . \qquad (22)$$

In the light of Eq. (15), we define the FLI with two-nearby-trajectories as follows:

$$\text{FLI}(\tau) = \log_{10} \frac{\| \Delta x(\tau) \|}{\| \Delta x(0) \|}. \qquad (23)$$

Next we shall mainly describe the numerical implementation of the FLI and test its validity in the description of dynamics.

B. The algorithm in detail

The original FLI proposed by Froeschlé and Lega [22] requires to compute the expansion rate of a tangential vector in the variational equations and it does not need any renormalization. We now reform it in general relativity into a coordinate invariant and compute it with the two particles approach. The FLI(τ) in Eq. (23) can not be computed without renormalization because the distance between the two particles, $\| \Delta x \|$, would expand so fast in the case of chaos as to it could reach the chaotic boundary to cause saturation.

In our numerical model (see the appendix) we choose $\| \Delta x(0) \| = 10^{-9}$. We found saturation when $\| \Delta x \| = 1$, therefore we choose $\| \Delta x \| = 0.1$ as the critical value to implement the renormalization. In this way, the number of renormalization for computing FLI is less than that for LE. This brings an advantage to guarantee the speed of computation. Let $k(k = 0, 1, 2, \cdots)$ be the sequential number of renormalization, then we calculate the FLI with the following expression:

$$\text{FLI}_k(\tau) = -k \cdot (1 + \log_{10} \| \Delta x(0) \|)$$
$$+ \log_{10} \frac{\| \Delta x(\tau) \|}{\| \Delta x(0) \|}, \qquad (24)$$

where $\| \Delta x(0) \| \leq \| \Delta x(\tau) \| \leq 0.1$. This technique depends on the choice of the initial deviation $\| \Delta x(0) \|$, and fails when $\| \Delta x(0) \|$ is too small or too large. After many numerical experiments, we found that $\| \Delta x(0) \| \approx 10^{-7}$–$10^{-9}$ works well.

C. Numerical tests of FLI

We take the initial separation $\Delta r = 10^{-9}$ and choose the regular orbit M and the chaotic one N in Fig. 1 to test the sensitivity of the FLI as well as Ψ. As is expected, Fig. 3 (colored light gray) displays that there is a drastic difference of the FLIs between the regular orbit and the chaotic one. For the ordered orbit, within a time span of 10^5 (equivalent to about 100 periods), the FLI is smaller than 1. However, we clearly see a sharp increase up to 24 of the FLI for the chaotic orbit. In other words, the length of the geodesic deviation vector $\boldsymbol{\xi}$ reaches the value 10^{24}. As mentioned above, the vector increases in an algebraic law for quasiperiodic orbits, but it does with an exponential law for chaotic orbits. Indeed the chaos of the orbit in the right of Fig. 3 becomes explicit after a time span 4.5×10^4. The FLI is a cheaper way to distinguish between chaotic and regular orbits and explore the global qualitative structure of the phase space of a system.

Another thing to emphasize is that the values of FLI are very analogous to that of Ψ (see black dots in Fig. 3). The values of FLIs by use of the two methods for the regular case have no difference in a long time since renormalization is not used. For the chaotic case we use only 2 times of renormalization. In general, it is enough to take small numbers of renormalization to calculate the FLIs in the orbits with weak chaos. This shows sufficiently the validity of our FLI with two-nearby-trajectories.

To examine the validity of the FLI further, in the left of Fig. 4 we have plotted the running maximum of FLIs as a function of the initial action r for a set of 1657 orbits that are regularly spaced in the interval [5.77, 22.34] on the axis $\dot{r} = 0$ in Fig. 1. Here each orbit is integrated until the time reaches 10^5. As is described in Fig. 1, the regular region is located in one interval between $R(8.45, 0)$ and $S(21, 0)$ and another interval between $R(22.15, 0)$ and the point (22.34, 0) on the straight line $\dot{r} = 0$. Obviously we find that all the FLIs in the two intervals are not larger than 6, but all the FLIs in the two intervals [5.77, 8.45] and [21, 22.14] on the
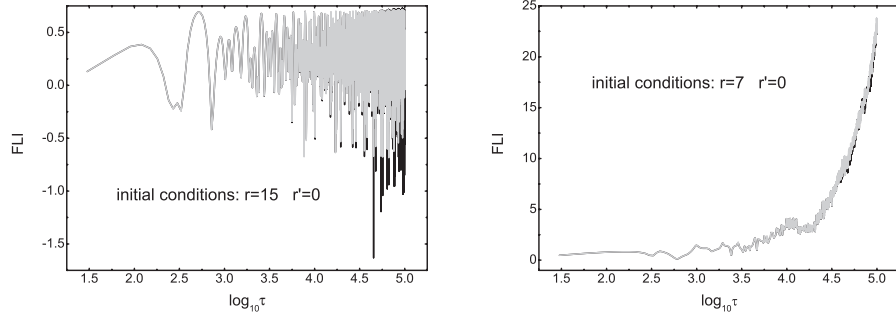
FIG. 3. The relation of FLIs with proper time by use of the index (23) for the regular orbit M in the left (colored light gray). The black dots correspond to the result obtained from Eq. (22). The right is the same as the left but for the chaotic orbit N in Fig. 1.
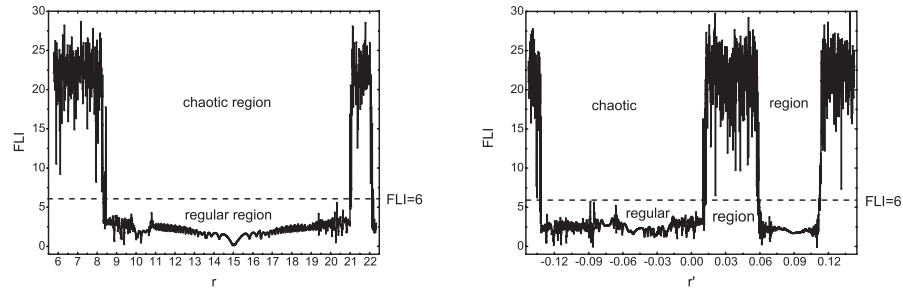

FIG. 4. Left: the evolution of the FLIs with the initial values of r ranging from the interval [5.77, 22.34] when the indicator (23) is used and $\dot{r} = 0$ is fixed at the initial time. Each orbit is integrated numerically till τ reaches 10^5. Two types of orbits consisting of regular and chaotic orbits are obtained according to distinct values of FLIs. Right: the same as the left, but $r = 9$ is fixed first, and $\dot{r}$ takes values from the interval $[-0.1428, 0.1428]$.

straight line $\dot{r} = 0$ are larger. This method displays the set of chaos, although it does not give the final values of LEs. In a similar way, the orbits along the straight line $r = 9$ in Fig. 1 are also separated into regular and chaotic intervals (see the right of Fig. 4). These facts show sufficiently that the FLI is rather successful to distinguish between the regularity and the chaoticity. However, we must point out a problem that the FLI does not provide more details about ordered orbits containing quasiperiodic and resonant periodic orbits. Here we give an illustration in detail.

On the basis of Froeschlé and Lega [22], the orbit with the starting point $M(15, 0)$ in Fig. 1 corresponds to a resonance since the maximum value of FLI arrives at about 0.68 as the smallest value in the left of Fig. 4. However this is not a resonant periodic orbit but just a quasiperiodic one. Actually the point $I(14.00349, -0.0312004)$ of the Poincaré map in the middle of tori is a fixed point. We found that all tori between the torus M and the point I have almost the same values of FLI. We cannot say that FLI is appropriate to identify the resonance categories. As another example, let us focus a trajectory made up of three little loops or islands surrounding three invariant points $J_1(9.0975, -0.0281)$, $J_2(17.13931, 0.04913)$ and $J_3(13.94246, -0.08936)$ in Fig. 1, respectively. An important point to mention lies in the manner where the three little loops appear on the plot as the same trajectory. Rather than tracing one loop at a time, successive points occur at

each of the three loops in turn. In this sense, the three fixed points are inhabited in the same periodic orbit. The maximum value of FLI we computed for this periodic (resonant) orbit after a time span of 10^5 turns out to be 1.75 or so. Obviously the value of FLI for the resonant orbit is larger than that for the quasiperiodic orbit M. In a word, it is difficult to apply values of FLI to distinguish various regular orbits.

D. Classification of orbits by FLI

Many experiments above have shown that our FLI is a very sensitive tool for detecting the regular and chaotic orbits. Next we shall follow this FLI to scan the global structure of phase space in the spacetime (A1). This operation is realized by calculating thousands of orbits in practice. First we fix $\dot{\theta} = 0$, meanwhile we let r run from $r_{min} = 5.77$ to $r_{max} = 22.34$ with a span of $\Delta r = 0.1$. Then, for each given r we can solve for $\dot{r}$ and find two roots $\dot{r}_-$ and $\dot{r}_+$ ($\dot{r}_- < 0$ and $\dot{r}_+ > 0$) from the Eq. (A4). Finally we take $\dot{r}$ from $\dot{r}_-$ to $\dot{r}_+$ with a sampling interval $\Delta \dot{r} = 0.01$. Once r and $\dot{r}$ are given initially, $\dot{\theta}$ should be derived by the relation (A4). As is shown in Fig. 5, we have plotted all the starting points on the $r - \dot{r}$ plane ($\theta = \pi/2$). According to different values of FLI, we classify orbits by some dynamical features. This is called as the description of the global structure of phase-space for the system.
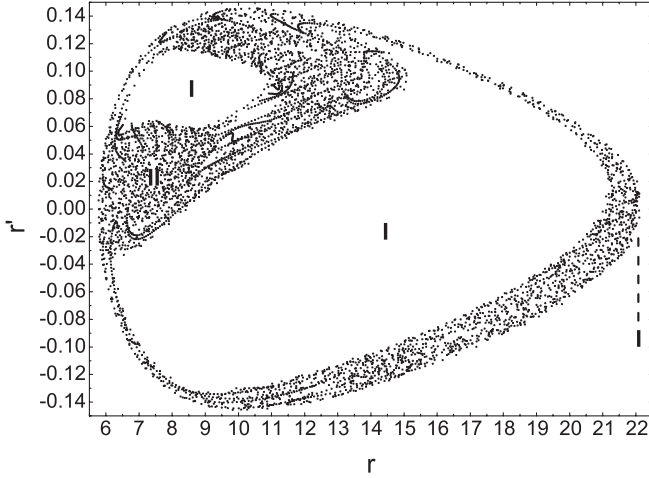
FIG. 5. Regions of different values of the FLIs on the plane $\theta = \frac{\pi}{2}$. Initial conditions are colored white if their FLIs ≤ 6, and black if FLIs > 6, which are corresponded to the regular region I, and chaotic region II, respectively. Here, all intersection points of an orbit with the plane should be regarded to have the same final value of the FLI.

By a comparison of Fig. 5 with Fig. 1, it is clear that the global dynamical features they depicted are nearly compatible. As an emphasis, an advantage to use FLI becomes more apparent because it applies to systems with an arbitrary number of dimensions. Without doubt, it is handy to study the global dynamics of the spinning compact binaries [10] by virtue of FLI. It is also easier to probe the variation of the dynamical characteristics as certain parameters of the system vary.

IV. SUMMARY

We compared three methods for computing LEs with coordinate gauge invariance in general relativity. The three methods are the geodesic deviation vector technique (M1), the two-nearby-orbits method with projection operations and with coordinate time as the integration independent variable (M2), and the two-nearby-orbits method without projection operations and with proper time as the integration independent variable (M3). The contributions of this work are as follows.

It is unnecessary to adopt the projection operators for M1 and M3 from the theoretical point of view. In addition, M2 works badly in some cases. As a result, M3 is the most preferable and worth to be recommended for the calculation of LEs in a relativistic gravitational system in most cases.

As another important contribution, we extended FLI to a coordinate invariant form in relativistic dynamics, and proposed its algorithm with the two-nearby-trajectories method. This indicator can rapidly, reliably and accurately distinguish between ordered and chaotic motions in relativistic astrophysics. Only when the initial separation and renormalization within a reasonable amount of time span are chosen appropriately, is this FLI nearly consistent with

the FLI computed with the geodesic deviation vector technique. However, the former is rather simpler to use than the latter. As a characteristic, our FLI grows exponentially with time in the chaotic case, while it grows algebraically in the case of quasiperiodic trajectories. Evaluating the different behaviors of this FLI, we successfully explored the global dynamics of phase space where regions of chaos and order are clearly identified.

It should be pointed out that a main advantage of the LE and FLI with two-nearby-trajectories is their easier application in treating complicated relativistic gravitational systems with high degrees of freedom, such as multibody problems and spinning compact binaries. In the future work, we shall employ an appropriate numerical integrator and the FLI to find out what happens in the spinning compact binaries. The global dynamics of the binary systems will be explored, and the transition from regular motion to chaos will be considered as some dynamical parameters of the system vary.

APPENDIX A: CORE-SHELL SYSTEM AND THE EQUATIONS OF MOTION

A Weyl spacetime including a nonrotating black hole surrounded by an axially symmetric shell in Schwarzchild coordinates (t, r, θ, ϕ) is expressed as [6]

$$ds^2 = -\left(1 - \frac{2}{r}\right)e^P dt^2 + e^{Q-P}\left[\left(1 - \frac{2}{r}\right)^{-1} dr^2 + r^2 d\theta^2\right] + e^{-P} r^2 \sin^2\theta d\phi^2, \tag{A1}$$

where P and Q are the functions of r and θ only. This system obviously has two integrals, the energy E and the angular momentum L in the forms

$$\dot{t} = Er(r - 2)^{-1} e^{-P}, \tag{A2}$$

$$\dot{\phi} = Le^P r^{-2} \sin^{-2}\theta. \tag{A3}$$

In addition, the 4-velocity of a particle always satisfies the constraint

$$U_\alpha U^\alpha = -\left(1 - \frac{2}{r}\right)e^P \dot{t}^2 + e^{Q-P}\left[\left(1 - \frac{2}{r}\right)^{-1}\dot{r}^2 + r^2\dot{\theta}^2\right]$$
$$+ e^{-P}r^2\sin^2\theta\dot{\phi}^2 = -1. \quad (A4)$$

If a fourth integral holds, the system is integrable. Otherwise, it is possible to yield chaos. However, it is not easy to deduce whether the fourth integral exists or not. To study the dynamics of a geodesic particle in this system further, we need the following geodesic equations

$$\ddot{r} = \left[\frac{1}{r(r-2)} + \frac{1}{2}\left(\frac{\partial P}{\partial r} - \frac{\partial Q}{\partial r}\right)\right]\dot{r}^2 - \left(\frac{\partial Q}{\partial \theta} - \frac{\partial P}{\partial \theta}\right)\dot{r}\dot{\theta}$$
$$+ (r-2)\left[1 + \frac{r}{2}\left(\frac{\partial Q}{\partial r} - \frac{\partial P}{\partial r}\right)\right]\dot{\theta}^2 + f_1(r, \theta), \quad (A5)$$

$$\ddot{\theta} = \frac{1}{2r(r-2)}\left(\frac{\partial Q}{\partial \theta} - \frac{\partial P}{\partial \theta}\right)\dot{r}^2 - \left(\frac{2}{r} + \frac{\partial Q}{\partial r} - \frac{\partial P}{\partial r}\right)\dot{r}\dot{\theta}$$
$$- \frac{1}{2}\left(\frac{\partial Q}{\partial \theta} - \frac{\partial P}{\partial \theta}\right)\dot{\theta}^2 + f_2(r, \theta), \quad (A6)$$

where

$$f_1(r, \theta) = -\frac{1}{2}\left(1 - \frac{2}{r}\right)e^{2P-Q}\left[\frac{2}{r^2} + \left(1 - \frac{2}{r}\right)\frac{\partial P}{\partial r}\right]\dot{t}^2$$
$$+ \frac{1}{2}(r-2)e^{-Q}\sin^2\theta \cdot \left(2 - r\frac{\partial P}{\partial r}\right)\dot{\phi}^2,$$

$$f_2(r, \theta) = -\frac{1}{2r^2}\left(1 - \frac{2}{r}\right)e^{2P-Q}\frac{\partial P}{\partial \theta}\cdot\dot{t}^2 + \frac{1}{2}e^{-Q}\cdot\sin\theta$$
$$\cdot\left(-\frac{\partial P}{\partial \theta}\sin\theta + 2\cos\theta\right)\dot{\phi}^2.$$

We now have to do the tedious derivation of the geodesic deviation equations. The result is too complex and will not be written here. If we take a' as the derivative of a with respect to coordinate time t, the above geodesic equations

are readjusted as follows:

$$r'' = \frac{\ddot{r}}{\dot{t}^2} - \frac{r'}{\dot{t}}\frac{d\dot{t}}{dt}, \quad (A7)$$

$$\theta'' = \frac{\ddot{\theta}}{\dot{t}^2} - \frac{\theta'}{\dot{t}}\frac{d\dot{t}}{dt}, \quad (A8)$$

$$\frac{d\dot{t}}{dt} = -Er(r-2)^{-1}e^{-P}\left(\frac{\partial P}{\partial r}r' + \frac{\partial P}{\partial \theta}\theta'\right)$$
$$- 2E(r-2)^{-2}e^{-P}r'.$$

Here $\dot{r}$ and $\dot{\theta}$ in Eqs. (A5) and (A6) should be changed into $\dot{r} = r'\dot{t}$ and $\dot{\theta} = \theta'\dot{t}$ respectively, while $\dot{t}$ and $\dot{\phi}$ remain the original expressions of Eqs. (A2) and (A3) because they do not contain coordinate time t explicitly.

Given two metric functions P and Q, the spacetime (A1) is determined at once. Now we reexamine the full relativistic core-shell configuration involving a Schwarzschild black hole plus a pure octopole shell studied by Vieira and Letelier [6]. In this model, we have

$$P(u, v) = \frac{1}{5}\mathcal{O}uv(5u^2 - 3)(5v^2 - 3),$$

$$Q(u, v) = -\frac{2}{5}\mathcal{O}v[5(3u^2 - 1)(1 - v^2) - 4]$$
$$+ \frac{3}{100}\mathcal{O}^2[-25u^6(1 - v^2)\cdot(5v^2 + 2v - 1)$$
$$\times (5v^2 - 2v - 1) + 15u^4(1 - v^2)$$
$$\times (65v^4 - 40v^2 + 3) - 3u^2(1 - v^2)(25v^2 - 3)$$
$$\times (5v^2 - 3) - v^2(25v^4 - 45v^2 + 27)],$$

where $u = r - 1$, $v = \cos\theta$, and $\mathcal{O}$ is an octopolar parameter.

[1] *Deterministic Chaos in General Relativity*, edited by D. Hobill, A. Burd, and A. Coley (Plenum Press, New York, 1994).
[2] F. Varadi, B. Runnegar, and M. Ghil, Astrophys. J. **592**, 620 (2003).
[3] L. F. Wanex, Ph.D. thesis, University of Nevada, 2002.
[4] G. Contopoulos, N. Voglis, and C. Efthymiopoulos, Celest. Mech. Dyn. Astron. **73**, 1 (1999).
[5] W. M. Vieira and P. S. Letelier, Phys. Lett. A **228**, 22 (1997).
[6] W. M. Vieira and P. S. Letelier, Astrophys. J. **513**, 383 (1999).
[7] M. D. Hartl and A. Buonanno, Phys. Rev. D **71**, 024027 (2005).
[8] M. D. Hartl, Phys. Rev. D **67**, 024005 (2003); Ph.D. thesis, California Institute of Technology, 2003.
[9] M. D. Hartl, Phys. Rev. D **67**, 104023 (2003).
[10] J. Levin, Phys. Rev. Lett. **84**, 3515 (2000).
[11] N. J. Cornish, Phys. Rev. D **64**, 084011 (2001).
[12] J. D. Schnittman and F. A. Rasio, Phys. Rev. Lett. **87**, 121101 (2001).
[13] N. J. Cornish and J. Levin, Phys. Rev. Lett. **89**, 179001 (2002).
[14] J. Levin, Phys. Rev. D **67**, 044013 (2003).
[15] N. J. Cornish and J. Levin, Phys. Rev. D **68**, 024004 (2003).
[16] M. Szydlowski, Gen. Relativ. Gravit. **29**, 185 (1997).
[17] G. Imponente and G. Montani, Phys. Rev. D **63**, 103501 (2001).
[18] G. Benettin, L. Galgani, and J.-M. Strelcyn, Phys. Rev. A **14**, 2338 (1976).
[19] Ch. Skokos, J. Phys. A **34**, 10029 (2001).

[20] Ch. Skokos, Ch. Antonopoulos, T. C. Bountis, and M. N. Vrahatis, J. Phys. A **37**, 6269 (2004).

[21] C. Froeschlé, E. Lega, and R. Gonczi, Celest. Mech. Dyn. Astron. **67**, 41 (1997).

[22] C. Froeschlé and E. Lega, Celest. Mech. Dyn. Astron. **78**, 167 (2000).

[23] X. Wu and T.-Y. Huang, Phys. Lett. A **313**, 77 (2003).

[24] G. Tancredi, A. Sánchez, and F. Roig, Astron. J. **121**, 1171 (2001).

[25] S. Udry and D. Pfenniger, Astron. Astrophys. **198**, 135 (1988).

[26] G. Contopoulos and B. Barbanis, Astron. Astrophys. **222**, 329 (1989).

[27] N. D. Caranicolas and N. J. Papadopoulos, New Astronomy **9**, 103 (2003).

[28] Y. Sota, S. Suzuki, and K. Maeda, Classical Quantum Gravity **13**, 1241 (1996).

[29] J. A. Nieto, J. Saucedo, and V. M. Villanueva, Phys. Lett. A **312**, 175 (2003).